

Structural and magnetic properties of $Tc_n@C_{60}$ endohedral metallofullerenes: First-principles predictions

Philippe F. Weck,^{1,*} Eunja Kim,² Kenneth R. Czerwinski,¹ and David Tománek^{3,†}

¹*Department of Chemistry and Harry Reid Center for Environmental Studies, University of Nevada Las Vegas, 4505 Maryland Parkway, Las Vegas, Nevada 89154, USA*

²*Department of Physics and Astronomy, University of Nevada Las Vegas, 4505 Maryland Parkway, Las Vegas, Nevada 89154, USA*

³*Physics and Astronomy Department, Michigan State University, East Lansing, Michigan 48824-2320, USA*

(Received 29 December 2009; published 31 March 2010)

We use *ab initio* spin-density-functional calculations to study the equilibrium structure and magnetic properties of $Tc_n@C_{60}$ endohedral metallofullerenes. We find that C_{60} can endohedrally accommodate Tc_n clusters with up to $n=7$ atoms, even though the encapsulation process becomes increasingly endothermic beyond $n=4$. The encapsulation does not change significantly the structure of the enclosed clusters, but reduces the magnetic moment due to a stronger Tc-C hybridization for the larger clusters.

DOI: [10.1103/PhysRevB.81.125448](https://doi.org/10.1103/PhysRevB.81.125448)

PACS number(s): 81.05.ub, 68.65.-k

I. INTRODUCTION

Endohedral metallofullerenes (EMFs), which consist of fullerene cages encapsulating metal atoms ($M@C_{2n}$), were identified¹ and isolated² shortly after the discovery of carbon fullerenes.³ Owing to their unique magnetic, electrical, and optical properties, EMFs are considered a promising class of nanostructures for materials and biomedical applications.^{2,4-9} In particular, radionuclide-filled EMFs have emerged in recent years as potentially valuable *in vivo* contrast agents and therapeutic radiopharmaceuticals, since they prevent undesired toxicity stemming from radionuclides catabolized by the host biological system.¹⁰⁻¹⁴ Radionuclide-filled EMFs possessing a net magnetic moment may be transported throughout the body using a weak inhomogeneous magnetic field, thus, allowing effective targeting of a tissue by the radiopharmaceuticals.¹⁵ In combination with the cytotoxic radiation dose delivered by the encapsulated radiometal, EMFs containing small clusters may also be used for therapy by hyperthermic killing of cancer cells, in analogy to gold nanoparticles.¹⁶

An additional application of fullerene cages is to serve as nanocontainers of radioactive isotopes for nuclear waste disposal¹⁷ owing to their unusually high thermal and mechanical stability that makes them resilient to radiation stemming from nuclear decay processes.¹⁸ The self-healing properties of fullerenes can also be regarded as beneficial in the event of a partial rupture of the carbon cage. Recent experimental findings have shown that radioactive nuclides as heavy as ²³⁸U or ²¹⁰Po can be encapsulated into C_{60} cages using standard arc/laser-induced vaporization methods¹⁹ or nuclear recoil implantation techniques.¹³

In this paper, we report *ab initio* calculations of the equilibrium structure, stability, and magnetic properties of $Tc_n@C_{60}$ isomers using density-functional theory (DFT). In particular, we assess the possibility of confining more than one Tc atom inside the fullerene cavity by calculating the encapsulation energy of Tc_n aggregates. We also map out the evolution of the total magnetic moment of Tc_n clusters upon encapsulation and the changing degree of Tc-C hybridization with increasing cluster size.

In comparison with other transition-metal elements of group VIIB, information on subnanometer Tc clusters is scarce.²⁰⁻²⁴ Reported *ab initio* results²³ for Tc_n clusters with up to $n=5$ atoms may be of questionable quality, since the reported $[Kr]4d^65s^1$ ground-state electronic configuration of the isolated Tc atom corresponds in reality to the lowest energy multiplet of the first excited state.²⁵

Despite the plethora of radionuclide-filled EMFs that have been either predicted or actually synthesized, to the best of our knowledge no metallofullerenes containing technetium atoms have been reported so far. This appears particularly surprising in light of the importance of technetium in the fields of nuclear waste management and nuclear medicine. Although technetium possesses no stable isotopes, its long-lived β^- -emitting isotope, ⁹⁹Tc ($t_{1/2}=2.13\times 10^5$ years, β^- =294 keV), is produced in sizable amounts from the nuclear fuel cycle (up to 6% fission yield) and constitutes an important challenge for environmental remediation.^{26,27} Additionally, ^{99m}Tc, its short-lived γ -emitting isotope originating from the decay of ⁹⁹Mo, is the most common isotope in diagnostic nuclear medicine (ca. 85% of all procedures) due to its optimal nuclear properties as a radioimaging agent ($t_{1/2}=6.02$ h, $\gamma=142$ keV).²⁸⁻³⁰

Hexagonal platelets of metallic Tc encapsulated into graphitic carbon shells were produced experimentally with a population distribution centered around 30–60 nm in diameter and 5 nm in thickness, and lattice parameters³¹ of $a_0=2.74(5)$ Å and $c_0=4.38(8)$ Å, close to the values of the hexagonal-closed-packed bulk Tc structure at ambient temperature and pressure³² (space group $P6_3/mmm$, $Z=2$, $a_0=2.7409\pm 0.0035$ Å, and $c_0=4.3987\pm 0.0034$ Å). However, the experimental identification and characterization of possible Tc-bearing EMFs remain elusive, in part due to their low solubility and extractability, or tedious separation procedures from other cage homologs. Therefore, first-principles calculations should provide useful insights into the search for EMFs containing Tc atoms.

Details of our computational approach are given in Sec. II, followed by a discussion of our results in Sec. III. A summary of our findings and conclusions are given in Sec. IV.

II. COMPUTATIONAL METHODS

First-principles total-energy calculations were performed using the spin-polarized density-functional theory as implemented in the Vienna *ab initio* simulation package (VASP).³³ The exchange-correlation energy was calculated using the generalized gradient approximation³⁴ (GGA), with the parametrizations of Perdew and Wang³⁵ (PW91) and Perdew, Burke, and Ernzerhof³⁶ (PBE). For transition-metal cluster computations, pure functionals such as the PW91 and PBE are generally preferred over hybrid functionals that appear to describe metal-metal bonds less accurately.^{37,38} In particular, the PW91 functional was found to correctly reproduce structural parameters of various Tc-containing molecules that had been characterized experimentally.^{39,40}

The interaction between valence electrons and ionic cores was described by the projector augmented wave (PAW) method.^{41,42} The Tc $4p^6 5s^2 4d^5$ and C $2s^2 2p^2$ electrons were treated explicitly as valence electrons in the Kohn-Sham (KS) equations and the remaining cores were represented by PAW pseudopotentials. The KS equations were solved using the blocked Davidson iterative matrix diagonalization scheme followed by the residual vector minimization method. The plane-wave cutoff energy for the electronic wave functions was set at 500 eV. A supercell approach was adopted in the calculations, with a large cubic cell with an edge length of 15 Å. Negligible interactions between molecular structures in adjacent unit cells warrant the adequacy of our Brillouin zone sampling scheme by a single k point at Γ . Geometries were optimized without symmetry constraints with the conjugate gradient method, accelerated using the Methfessel-Paxton Fermi-level smearing⁴³ with a Gaussian width of 0.1 eV. The total energy of the molecular system and Hellmann-Feynman forces acting on atoms were calculated with convergence tolerances set to 10^{-3} eV and 0.01 eV/Å, respectively. The analysis of the charge density of the relaxed EMF structures was carried out using the DMOL3 software.⁴⁴

III. RESULTS AND DISCUSSION

Optimized geometries of the lowest-energy structures of free Tc_n clusters ($n=2-7$), calculated at the GGA/PW91 level of theory, are displayed in Fig. 1, along with their corresponding bond distances, total spin, and point group symmetry. Our calculated structures are in fair overall agreement with geometries recently predicted by nonmagnetic DFT calculations.²⁴ However, including the additional spin degrees of freedom leads to symmetry reduction in many clusters. Similar to other transition-metal clusters, structural Jahn-Teller-like distortions can be viewed as an attempt to restore collinearity of the spin moments.⁴⁵

The electronic ground state of the Tc dimer has a triplet configuration, with the calculated equilibrium bond length of $R_e = 1.84$ Å. This is in line with the recent multiconfiguration second-order perturbation theory prediction⁴⁶ of a $X^3\Sigma_g^-$ electronic ground state with a strong quintuple bond ($R_e = 1.939$ Å) for Tc_2 . This result is, however, in strong contrast with the dimer of Mn, also a group VIIB transition

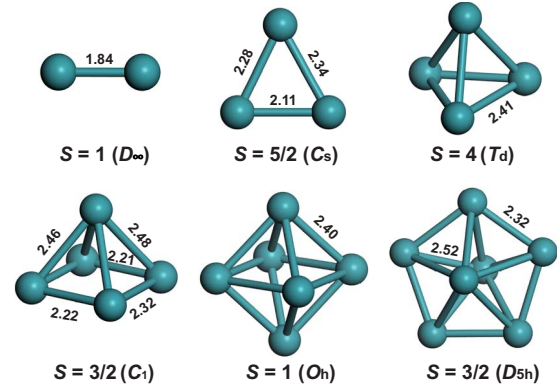


FIG. 1. (Color online) Ball-and-stick models of the equilibrium structures of free Tc_n ($n=2-7$) clusters computed at the GGA/PW91 level of theory. Additional information listed includes the calculated bond distances (in angstrom), total spin, and point-group symmetry.

metal, which forms a weakly bound van der Waals complex due to its large $3d^5 4s^2 \rightarrow 3d^6 4s^1$ excitation energy that prevents orbital hybridization.⁴⁷

The most stable structure of Tc_3 is a triangle with C_s symmetry and side lengths ranging between 2.11–2.34 Å corresponding to a sextet state. The three-dimensional cluster growth regime starts with Tc_4 , which forms a regular tetrahedron with edges of 2.41 Å in its nonet electronic ground state. Tc_5 , which possesses a quartet multiplicity in its ground state, adopts a strongly distorted pyramidal geometry with bond lengths ranging from 2.21 to 2.48 Å. This represents a noticeable departure from the D_{3h} trigonal bipyramidal structure predicted²⁴ for the lowest-lying singlet state of Tc_5 .

Tc_6 prefers a regular octahedral structure, with Tc-Tc bonds of 2.40 Å, over other possible isomers with reduced symmetries in the triplet ground state. A pentagonal bipyramid with D_{5h} symmetry and bond lengths of 2.32 and 2.52 Å is the lowest-energy isomer of Tc_7 that corresponds to a quartet state. The equilibrium cluster structures computed using the PBE functional are essentially identical with those obtained using PW91, with differences in corresponding bond lengths of typically less than 0.005 Å.

The equilibrium structure of the $Tc_n@C_{60}$ ($n=2-7$) endohedral metalfullerenes and the frozen substructure of the encapsulated Tc_n clusters, calculated at the GGA/PW91 level of theory, are depicted in Fig. 2. Only minute differences were found between the equilibrium structures calculated using the PBE and PW91 functionals. For a single encapsulated Tc atom, the C_{60} cage preserves its structure including icosahedral symmetry due to the weak interaction between the centrally located metal atom and the surrounding carbon atoms.

The $Tc_2@C_{60}$ EMF adopts the C_{3v} symmetry as a whole, with Tc_2 oriented preferentially along a S_6 symmetry axis of the C_{60} and with a Tc-Tc bond length of 1.82 Å, slightly shorter than in the isolated dimer. The structural evolution of encapsulated Tc_n clusters from $n=3$ to $n=7$ follows a growth pathway similar to Mn clusters.⁴⁸ Two Tc atoms of the encapsulated Tc_3 cluster with C_s symmetry are coordinated to

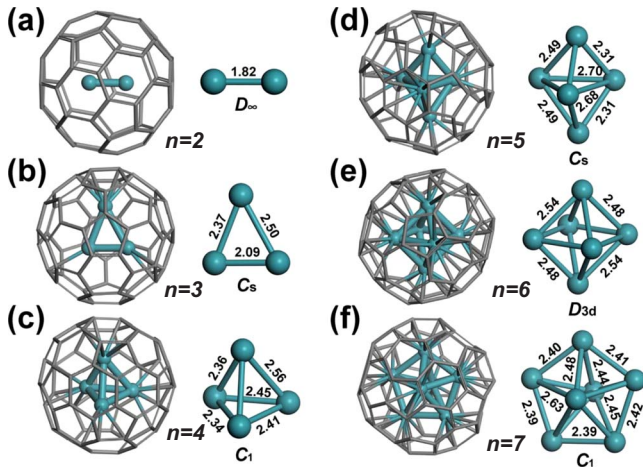


FIG. 2. (Color online) Ball-and-stick models of the equilibrium structure of $Tc_n@C_{60}$ endohedral metallofullerenes (left) and the frozen substructure of the encapsulated Tc_n clusters (right) calculated at the GGA/PW91 level of theory. Additional information listed includes the calculated bond distances (in angstrom) and point-group symmetry of the encapsulated clusters.

hexagonal rings with η^6 and η^3 hapticities; the third Tc atom forms a single bond with the carbon cage. Upon encapsulation, Tc_4 becomes strongly distorted, with Tc-Tc bond lengths in the range from 2.34 to 2.56 Å.

The most significant structural transformation occurs for Tc_5 , which undergoes a transition from a distorted tetragonal pyramid to a trigonal bipyramid with C_s symmetry upon encapsulation. The equilibrium structure of $Tc_6@C_{60}$ possesses a D_{3d} symmetry imposed by the encapsulated metal cluster, which undergoes a distortion with respect to the free Tc_6 octahedron. Tc-Tc bond lengths are also slightly elongated (2.48 and 2.54 Å) in the encapsulated Tc_6 cluster as a result of the Tc-C hybridization. The most stable structure of $Tc_7@C_{60}$ is asymmetric, with the approximate S_5 symmetry axis of the distorted pentagonal bipyramid oriented along a pentagon-pentagon axis of the fullerene. Both apex atoms of the Tc_7 bipyramid are coordinated to pentagonal carbon rings with η^5 hapticity. We found all $Tc_n@C_{60}$ isomers with $n > 7$ to be unstable and to disintegrate spontaneously.

To identify encapsulated metallofullerenes that may form under synthesis conditions, we first define the encapsulation energy ΔE_n as the energy gain in the $Tc_n + C_{60} \rightarrow Tc_n@C_{60}$ reaction. We define

$$\Delta E_n = E(Tc_n@C_{60}) - E(Tc_n) - E(C_{60}), \quad (1)$$

where $E(Tc_n@C_{60})$, $E(Tc_n)$, and $E(C_{60})$ are the total energies of the Tc-containing EMFs and their constituents. The evolution of the computed encapsulation energy as a function of the cluster size is presented in Fig. 3. Our results indicate that encapsulation energy values calculated using the PW91 and PBE energy functionals are very close. Consequently, we will use PW91 results in the following discussion.

The encapsulation of a single Tc atom is slightly endothermic, with $\Delta E_1 = +0.19$ eV. The Tc dimer is even less likely to be encapsulated, since the positive encapsulation energy $\Delta E_2 = +0.78$ eV is even larger. A similar trend was

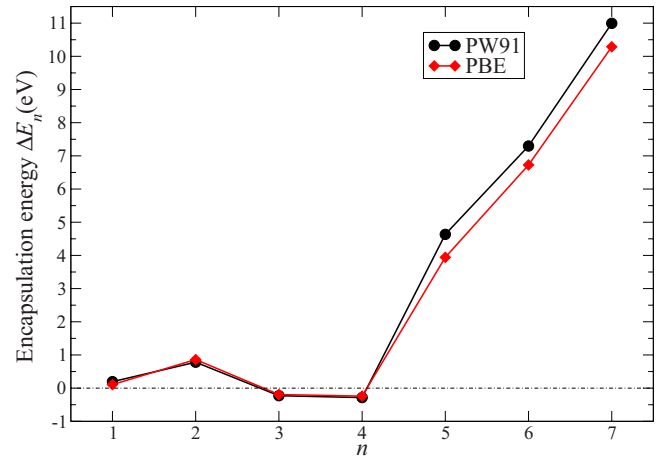


FIG. 3. (Color online) Dependence of the encapsulation energy ΔE_n , associated with the $Tc_n + C_{60} \rightarrow Tc_n@C_{60}$ reaction, on the cluster size n .

reported recently⁴⁹ for the encapsulation of Fe and Fe_2 inside C_{60} . The formation of $Tc_3@C_{60}$ and $Tc_4@C_{60}$ is predicted to be exothermic with $\Delta E_3 = -0.22$ eV and $\Delta E_4 = -0.28$ eV. This reflects the stabilization enhancement of the EMFs caused by the creation of Tc-C bonds. The encapsulation process becomes strongly endothermic beyond $n=4$. We find $\Delta E_n > 4$ eV, with a near-linear dependence of the encapsulation energy on the cluster size n . Therefore, the probability to produce $Tc_n@C_{60}$ EMFs with encapsulated clusters larger than Tc_4 appears rather small from an energetic viewpoint.

In Fig. 4 we plot the total electronic magnetic moment μ of free Tc_n clusters and of $Tc_n@C_{60}$ EMFs, obtained using the PW91 and PBE functionals, as a function of the cluster size n . A nonzero magnetic moment is rather unexpected in these systems in view of the fact that Tc is nonmagnetic as bulk metal,⁵⁰ with weak paramagnetism only occurring when in contact with a system containing unpaired electrons in the highest occupied level.⁵¹ Unlike in the free Tc_n clusters, with the exception of $n=1$ and $n=3$, the calculated magnetic mo-

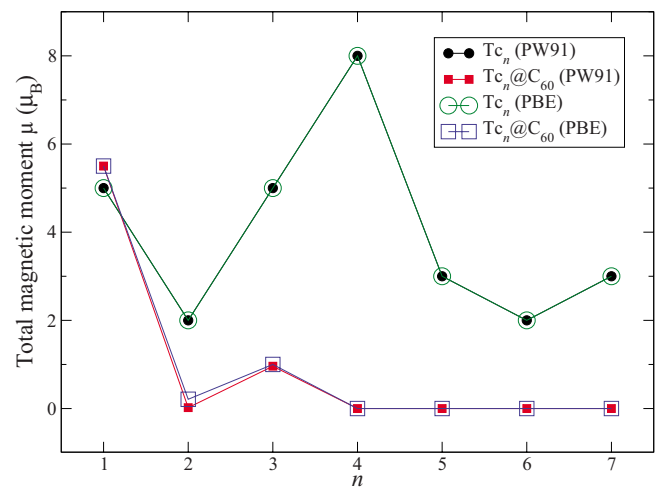


FIG. 4. (Color online) Dependence of the total electronic magnetic moment μ in free Tc_n clusters and in $Tc_n@C_{60}$ endohedral metallofullerenes on the cluster size n .

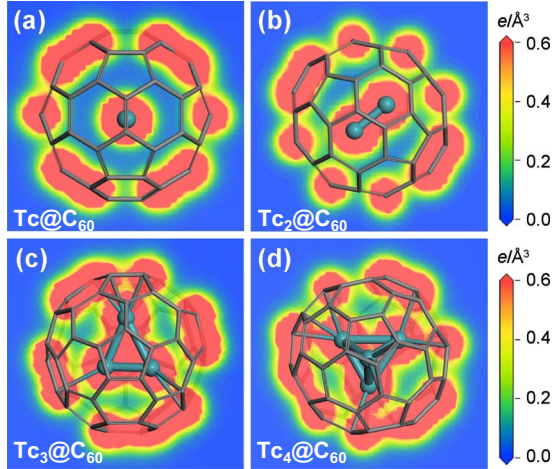


FIG. 5. (Color online) Cross sections of the total electron charge density ρ of (a) $\text{Tc}@C_{60}$, (b) $\text{Tc}_2@C_{60}$, (c) $\text{Tc}_3@C_{60}$, and (d) $\text{Tc}_4@C_{60}$. The charge density is computed at the GGA/PW91 level of theory and plotted in $e/\text{\AA}^3$ units.

ment of $\text{Tc}_n@C_{60}$ EMFs is zero. The reason for the suppression of the magnetic moment in large encapsulated Tc_n clusters lies in the formation of covalent bonds between Tc atoms and the C shell atoms. This is best illustrated in the charge-density plots for various EMFs displayed in Figs. 5(a)–5(c).

The magnetic moment $\mu=5.5 \mu_B$ of $\text{Tc}@C_{60}$, larger by $0.5 \mu_B$ than that of the free Tc atom, may be caused by small global sphere currents in the C_{60} shell following the encapsulation. Such currents arise from the motion of the delocalized π electrons across the entire surface of the buckminsterfullerene.⁵² The calculated Hirshfeld charge of $+0.24e$ on the encapsulated Tc atom suggests that part of its valence electrons have been transferred to the carbon host. Even though no Tc-C covalent bonds are created in $\text{Tc}_2@C_{60}$, a significant interaction between the dimer and the cage can be inferred due to the drastic reduction in the total magnetic moment upon encapsulation. This is further corroborated by the presence of a $0.2\text{--}0.4 e/\text{\AA}^3$ electron charge density found in the interstitial region between each of the Tc atoms and the hexagonal carbon rings at the poles as seen in Fig. 5(b). The computed Hirshfeld charge of $+0.30e$ carried by the encapsulated dimer ($+0.15e$ per Tc atom) also shows an increase in the electron charge transferred to C_{60} .

Even though the net magnetic moment of $\text{Tc}_3@C_{60}$ does not vanish, its value $\mu=1.0 \mu_B$ is also reduced with respect to the free cluster due to the hybridization between Tc $4d$ and C $2p$ orbitals. The two Tc atoms of the encapsulated Tc_3 cluster that are coordinated to hexagonal rings with η^6 and η^3 hapticities carry the net charges of $+0.12e$ and $+0.10e$. The third Tc atom, which forms a single bond with the carbon cage, carries a smaller charge of $+0.09e$. Differences in

the chemical interaction of these Tc atoms with the carbon host can be clearly seen in Fig. 5(c).

The total magnetic moment of $\text{Tc}_4@C_{60}$, the heaviest EMF that is stable against decomposition into Tc_4 and C_{60} , vanishes due to the efficient Tc-C hybridization, depicted in Fig. 5(d). The calculated net Hirshfeld charge of $+0.35e$ for the entire Tc_4 is nearly equipartitioned across the Tc atoms, which each carry a charge in the range from $+0.08\text{--}0.09e$.

IV. SUMMARY AND CONCLUSIONS

We have studied the equilibrium structure and magnetic properties of $\text{Tc}_n@C_{60}$ endohedral metallofullerenes using *ab initio* spin-density-functional theory. Our results indicate that C_{60} can endohedrally accommodate Tc_n clusters with up to $n=7$ atoms, although the encapsulation process becomes increasingly endothermic beyond $n=4$. The encapsulation does not change significantly the structure of the enclosed clusters, except for Tc_5 that undergoes a transition from a distorted tetragonal pyramid to a trigonal bipyramid with C_s symmetry upon encapsulation. Only an isolated Tc atom is predicted to maintain its net magnetic moment upon encapsulation, whereas the magnetic moment of larger Tc_n clusters is reduced upon encapsulation due to an efficient Tc-C hybridization.

$\text{Tc}_n@C_m$ metallofullerenes may contain C_m cages larger than the C_{60} fullerene, but the experimental identification of such systems is more complex. Whereas the arrangement of pentagons and hexagons satisfying the isolated-pentagon rule (IPR) is unique in C_{60} , higher fullerenes have more than one IPR-compliant isomer. Moreover, the IPR is often violated in metallofullerenes, thus, further increasing the number of viable isomer structures, which provides additional complications for structural characterization. Furthermore, exohedral functionalization of the fullerene surface⁵³ for optimum radiopharmaceutical and nuclear waste disposal applications is also likely to affect the structural and magnetic properties of these EMFs. More calculations are needed in order to support experimental studies aimed at identifying Tc-containing EMFs with larger or chemically functionalized cages and studying their structure, stability, reactivity, and magnetic properties.

ACKNOWLEDGMENTS

This project was funded under the auspices of the U.S. Department of Energy, Office of Nuclear Energy, Cooperative Agreement No. DE-FG07-01AL67358. Funding for this research was also provided by a subcontract through Battelle 0089445 from the U.S. Department of Energy, Agreement No. DE-AC07-05ID14517. D.T. was funded by the National Science Foundation under NSF-NSEC Grant No. 425826 and NSF-NIRT Grant No. ECS-0506309.

*weckp@unlv.nevada.edu

†tomanek@msu.edu

- ¹J. R. Heath, S. C. O'Brien, Q. Zhang, Y. Liu, R. F. Curl, H. W. Kroto, F. K. Tittel, and R. E. Smalley, *J. Am. Chem. Soc.* **107**, 7779 (1985).
- ²Y. Chai, T. Guo, C. M. Jin, R. E. Haufler, L. P. F. Chibante, J. Fure, L. H. Wang, J. M. Alford, and R. E. Smalley, *J. Phys. Chem.* **95**, 7564 (1991).
- ³H. W. Kroto, J. R. Heath, S. C. O'Brien, R. F. Curl, and R. E. Smalley, *Nature (London)* **318**, 162 (1985).
- ⁴D. S. Bethune, R. D. Johnson, J. R. Salem, M. S. Devries, and C. S. Yannoni, *Nature (London)* **366**, 123 (1993).
- ⁵F. T. Edelmann, *Angew. Chem., Int. Ed. Engl.* **34**, 981 (1995).
- ⁶T. Nakane, Z. Xu, E. Yamamoto, T. Sugai, T. Tomiyama, and H. Shinohara, *Fullerene Sci. Technol.* **5**, 829 (1997).
- ⁷H. Shinohara, *Rep. Prog. Phys.* **63**, 843 (2000).
- ⁸M. Takata, E. Nishibori, M. Sakata, and H. Shinohara, *Struct. Chem.* **14**, 23 (2003).
- ⁹S. Guha and K. Nakamoto, *Coord. Chem. Rev.* **249**, 1111 (2005).
- ¹⁰M. Mikawa, H. Kato, M. Okumura, M. Narazaki, Y. Kanazawa, N. Miwa, and H. Shinohara, *Bioconjugate Chem.* **12**, 510 (2001).
- ¹¹E. B. Iezzi, J. C. Duchamp, K. R. Fletcher, T. E. Glass, and H. C. Dorn, *Nano Lett.* **2**, 1187 (2002).
- ¹²R. D. Bolskar, A. F. Benedetto, L. O. Husebo, R. E. Price, E. F. Jackson, S. Wallace, L. J. Wilson, and J. M. Alford, *J. Am. Chem. Soc.* **125**, 5471 (2003).
- ¹³T. Ohtsuki and K. Ohno, *Phys. Rev. B* **72**, 153411 (2005).
- ¹⁴M. D. Diener, J. M. Alford, S. J. Kennel, and S. Mirzadeh, *J. Am. Chem. Soc.* **129**, 5131 (2007).
- ¹⁵M. Yoon, P. Borrmann, and D. Tománek, *J. Phys.: Condens. Matter* **19**, 086210 (2007).
- ¹⁶S. Lal, S. E. Clare, and N. J. Halas, *Acc. Chem. Res.* **41**, 1842 (2008).
- ¹⁷I. Amato, *Science* **258**, 1886 (1992).
- ¹⁸F. Cataldo, G. Strazzulla, and S. Iglesias-Groth, *Mon. Not. R. Astron. Soc.* **394**, 615 (2009).
- ¹⁹M. D. Diener, C. A. Smith, and D. K. Veirs, *Chem. Mater.* **9**, 1773 (1997).
- ²⁰E. Hartmann and G. Seifert, *Phys. Status Solidi B* **100**, 589 (1980).
- ²¹V. P. Tarasov, Y. B. Muravlev, K. E. German, and N. N. Popova, *Dokl. Phys. Chem.* **337**, 71 (2001) [*Dokl. Akad. Nauk* **337**, 221 (2001)].
- ²²M. Defranceschi and G. Berthier, *J. Nucl. Mater.* **304**, 212 (2002).
- ²³R. Sekine, R. Kondo, T. Yamamoto, and J. Onoe, *Radiochem.* **45**, 233 (2003).
- ²⁴P. F. Weck, E. Kim, F. Poineau, and K. R. Czerwinski, *Phys. Chem. Chem. Phys.* **11**, 10003 (2009).
- ²⁵J. A. Rard, M. H. Rand, J. R. Thornback, and H. Wanner, *J. Chem. Phys.* **94**, 6336 (1991).
- ²⁶K. H. Lieser, *Radiochim. Acta* **63** (Special Issue), 5 (1993).
- ²⁷A. Maes, K. Geraedts, C. Bruggeman, J. Vancluysen, A. Rossberg, and C. Hennig, *Environ. Sci. Technol.* **38**, 2044 (2004).
- ²⁸K. Schwochau, *Technetium: Chemistry and Radiopharmaceutical Applications* (Wiley-VHC, New York, 2000).
- ²⁹T. Storr, K. H. Thompson, and C. Orvig, *Chem. Soc. Rev.* **35**, 534 (2006).
- ³⁰F. Tisato, M. Porchia, C. Bolzati, F. Refosco, and A. Vittadini, *Coord. Chem. Rev.* **250**, 2034 (2006).
- ³¹T. J. Senden, K. H. Mook, J. D. Fitz Gerald, W. M. Burch, R. J. Browitt, C. D. Ling, and G. A. Heath, *J. Nucl. Med.* **38**, 1327 (1997).
- ³²J. A. Rard, M. H. Rand, G. Andregg, and H. Wanner, *Chemical Thermodynamics of Technetium*, Chemical Thermodynamics Vol. 3, edited by M. C. A. Sandino and E. Ostholts (OECD Nuclear Energy Agency, Data Bank, Issy-les-Moulineaux, France, 1999).
- ³³G. Kresse and J. Furthmüller, *Phys. Rev. B* **54**, 11169 (1996).
- ³⁴J. P. Perdew, J. A. Chevary, S. H. Vosko, K. A. Jackson, M. R. Pederson, D. J. Singh, and C. Fiolhais, *Phys. Rev. B* **46**, 6671 (1992).
- ³⁵J. P. Perdew and Y. Wang, *Phys. Rev. B* **45**, 13244 (1992).
- ³⁶J. P. Perdew, K. Burke, and M. Ernzerhof, *Phys. Rev. Lett.* **77**, 3865 (1996).
- ³⁷G. L. Gutsev and J. C. W. Bauschlicher, *J. Phys. Chem. A* **107**, 7013 (2003).
- ³⁸F. Furche and J. P. Perdew, *J. Chem. Phys.* **124**, 044103 (2006).
- ³⁹P. F. Weck, E. Kim, F. Poineau, E. Rodriguez, A. P. Sattelberger, and K. R. Czerwinski, *Inorg. Chem.* **48**, 6555 (2009).
- ⁴⁰F. Poineau, P. F. Weck, P. Forster, A. P. Sattelberger, and K. R. Czerwinski, *Dalton Trans.* **2009**, 10338.
- ⁴¹P. E. Blöchl, *Phys. Rev. B* **50**, 17953 (1994).
- ⁴²G. Kresse and D. Joubert, *Phys. Rev. B* **59**, 1758 (1999).
- ⁴³M. Methfessel and A. T. Paxton, *Phys. Rev. B* **40**, 3616 (1989).
- ⁴⁴B. Delley, *J. Chem. Phys.* **113**, 7756 (2000).
- ⁴⁵G. Rollmann, P. Entel, and S. Sahoo, *Comput. Mater. Sci.* **35**, 275 (2006).
- ⁴⁶A. C. Borin, J. P. Gobbo, and B. O. Roos, *Mol. Phys.* **107**, 1035 (2009).
- ⁴⁷M. D. Morse, *Advances in Metal and Semiconductor Clusters* (JAI Press Inc., Greenwich, CT, 1993), Vol. 1.
- ⁴⁸G. L. Gutsev, M. D. Mochena, and J. C. W. Bauschlicher, *J. Phys. Chem. A* **110**, 9758 (2006).
- ⁴⁹G. Gao and H. S. Kang, *Chem. Phys. Lett.* **462**, 72 (2008).
- ⁵⁰V. L. Moruzzi and P. M. Marcus, *Phys. Rev. B* **48**, 7665 (1993).
- ⁵¹V. P. Tarasov, Y. B. Muravlev, and K. E. Guerman, *J. Phys.: Condens. Matter* **13**, 11041 (2001).
- ⁵²M. P. Johansson, J. Jusélius, and D. Sundholm, *Angew. Chem., Int. Ed.* **44**, 1843 (2005).
- ⁵³E. Kim, P. F. Weck, S. Berber, and D. Tománek, *Phys. Rev. B* **78**, 113404 (2008).